Detection of Leukocytes in Contact with the Vessel Wall from *In Vivo* Microscope Recordings Using a Neural Network

M. Egmont-Petersen*, U. Schreiner, S. C. Tromp, T. M. Lehmann, *Member, IEEE*, D. W. Slaaf, and T. Arts

***Abstract*—Leukocytes play an important role in the host defense as they may travel from the blood stream into the tissue in reacting to inflammatory stimuli. The leukocyte-vessel wall interactions are studied in post capillary vessels by intravital video microscopy during *in vivo* animal experiments. Sequences of video images are obtained and digitized with a frame grabber. A method for automatic detection and characterization of leukocytes in the video images is developed. Individual leukocytes are detected using a neural network that is trained with synthetic leukocyte images generated using a novel stochastic model. This model makes it feasible to generate images of leukocytes with different shapes and sizes under various lighting conditions. Experiments indicate that neural networks trained with the synthetic leukocyte images perform better than networks trained with images of manually detected leukocytes. The best performing neural network trained with synthetic leukocyte images resulted in an 18% larger area under the ROC curve than the best performing neural network trained with manually detected leukocytes.**

***Index Terms*—Leukocyte detection, microcirculation, model-based image processing, nonlinear filtering, object recognition, shape characterization, stochastic model.**

I. Introduction

LEUKOCYTES (white blood cells) play an important role in the host defense. In reacting to inflammatory stimuli, leukocytes may travel from the blood stream into the tissue. Initially, leukocytes marginate and roll along the wall of venules with a low velocity as compared to the surrounding erythrocytes (red blood cells). The leukocyte-vessel wall interactions can be studied by intravital microscopy during *in vivo* animal experiments [1].

It is our objective to develop an approach for detection and tracking of individual leukocytes in sequences of video images from *in vivo* microcirculation experiments. Our first goal is to automatically detect leukocytes in microscopic video sequences and characterize their size and shape. This goal is not fulfilled by existing approaches for offline analysis of microcirculation images which were developed specifically for automatically estimating the velocity of moving leukocytes [2] or erythrocytes [3]–[5]. As none of these approaches determines the exact position of the blood cells in each image, the size and shape of each cell cannot be characterized precisely.

In [6], several approaches for object recognition were compared. One type of approaches is based on linear [7] or nonlinear filtering by convolution [8], another type of approaches on feature-based classifiers [9], [10]. Contour-based approaches (snakes [11]–[13], point distribution models [14] and the Hough transform [7]) constitute a third category. Only methods based on filtering or on recognition by query [15], [16] use the complete intensity distribution of the convolution window. So we decided to train a statistical classifier to detect the leukocytes by convolution.

Several statistical classifiers could be trained to recognize objects from the intensity distribution in a convolution window. As stated in [10], a feed-forward neural network with one hidden layer is a nonlinear classifier that is capable of fitting any discriminant function when provided with a sufficient number of hidden nodes [17]–[19]. It has, furthermore, been proven that training a feed-forward neural network with a sufficient number of representative learning cases results in a Bayes-optimal nonlinear filter [8], [20]. So we develop a neural-network-based approach for detection of leukocytes, which obtains as input the intensities of the pixels of a quadratic window. The weights of the network need to be trained with a statistically representative training set to distinguish leukocytes from the heterogeneous background in the blood vessel mainly consisting of rapidly moving erythrocytes. For this purpose, we develop a stochastic model of the intensity distribution of a leukocyte. By varying the model parameters simultaneously, we are able to generate synthetic images of leukocytes with a realistic diversity in cell size, shape, membrane contrast, and inner and outer texture. These images are used to compose a training set for the neural network.

The paper is organized as follows. First, we describe the physiological background that motivates the automatic detection of leukocytes. The visual appearance of leukocytes in our image material (their shape, contrast, and texture) is subsequently analyzed in detail. The results from this analysis are used to build a stochastic model for generation of synthetic leukocyte images. Experiments are conducted to investigate whether feed-forward neural networks can be trained to detect

Manuscript received June 22, 1999; revised February 15, 2000. *Asterisk indicates corresponding author.*

*M. Egmont-Petersen is with the Department of Biophysics, Maastricht University, Maastricht, The Netherlands (e-mail: michael@lkeb.azl.nl).

U. Schreiner is with the Department of Biophysics, Maastricht University, Maastricht, The Netherlands. He is also with the Institute of Medical Informatics, Aachen University of Technology, Aachen, Germany.

S. C. Tromp is with the Department of Physiology, Maastricht University, Maastricht, The Netherlands.

T. M. Lehmann are with the Institute of Medical Informatics, Aachen University of Technology, Aachen, Germany.

D. W. Slaaf and T. Arts are with the Department of Biophysics, Maastricht University, Maastricht, The Netherlands.

Publisher Item Identifier S 0018-9294(00)05135-1.

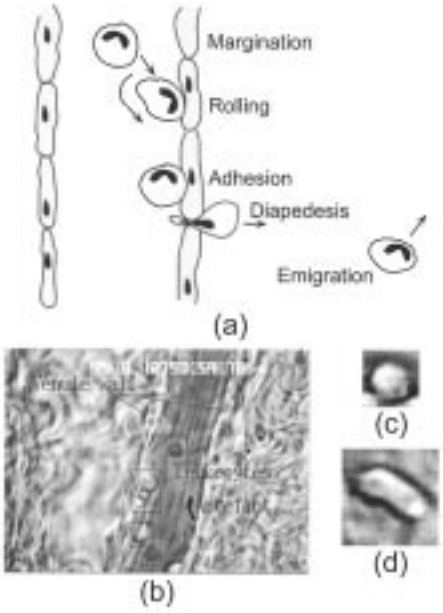

Fig. 1. (a) Overview of the several steps, margination, rolling, adhesion, diapedesis, and emigration, from free flowing leukocyte to migration into inflamed tissue. (b) Video image obtained from an *in vivo* experiment in a rabbit. It shows a post capillary venule in a prepared mesentery. (c) A typical interacting leukocyte. (d) A (seldomly observed) interacting leukocyte with a banana shape.

leukocytes in microcirculation images. The performance of the neural networks trained with real and artificially generated leukocyte images is compared.

II. Analysis of Leukocyte Images

A. Physiological Background

In case of inflammation or as a reaction to mechanical trauma, leukocytes tend to migrate into the surrounding tissue. This process consists of several consecutive steps [21] [Fig. 1(a)]: margination toward the vessel wall, weak interaction with the endothelium (rolling), strong activation and adhesion, which is eventually followed by diapedesis where the leukocytes pass the interstice between two neighboring endothelial cells that concomitantly contract. In our research, especially the rolling step is studied [Fig. 1(c) shows a magnification of a typical leukocyte that interacts with the vessel wall]. Leukocytes roll with a relatively slow velocity along the vessel wall section.

During their interaction with the vessel wall, the shape of the leukocytes changes. The forces exerted on a cell, the degree of adhesion and the degree of activation of the endothelium determine in concert the ellipticity and rotational speed of individual leukocytes as well as the number of leukocytes concomitantly sticking to the venule wall.

Venules within the mesentery of rabbits and rats [see Fig. 1(b)] were visualized with a Leitz intravital microscope, adapted for telescopic imaging [22] using a Leitz water-immersion objective (SW25, numerical aperture 0.60). The mid plane of the vessel—where the diameter is maximal—is kept in focus during the experiment. Transillumination was performed with a tungsten lamp. Final magnification at the front plane of the camera was $\times 52$. Images were recorded on VCR and grabbed with a frame grabber from data translation at a frequency of 25 Hz. The images were separated into fields (odd and even video lines which entail a sampling frequency of 50 Hz) and blurred with an elliptic Gaussian kernel ($\sigma^2_{\text{horz}} = 1$, $\sigma^2_{\text{vert}} = 1/2$ [23]). The field images were then subsampled with a factor 2 in the horizontal direction such that the horizontal and vertical scales become identical.

Before a realistic model of the intensity distribution of a leukocyte can be built, it is necessary to analyze the appearance of leukocytes in our video image sequences. A leukocyte is enveloped by a cell membrane which appears as a band darker than both the cell cytoplasm and the surroundings of the cell. This so-called envelope band has the following features:

1) its circumference in pixels;
2) its round or elliptic shape;
3) the texture of the envelope band.

The cytoplasm of a leukocyte is characterized by a texture with a frequency spectrum that deviates considerably from that of the surrounding (fast-moving) erythrocytes, especially along the direction of flow where the fast erythrocyte motion caused by the blood stream entails a spectrum prevailed by low frequencies. Finally, the average intensity of the cytoplasm texture deviates from the average intensity of the erythrocytes that surround the leukocytes in the blood vessel.

B. Elliptic Contour

In the image sequences, the membrane of most adhering leukocytes has an elliptic shape so we choose the ellipse as the basic model of the contour of a leukocyte. The coordinates of an ellipse[1] $\boldsymbol{c} = (x, y)^{\mathrm{T}}$ are defined implicitly by

$$\boldsymbol{c}^{\mathrm{T}} \Lambda \boldsymbol{c} = 1 \tag{1}$$

with Λ a diagonal matrix containing the two nonzero diagonal elements λ_1 and λ_2. The length (in pixels) of the long and short axes of the ellipse is given by λ_1^{-2} and λ_2^{-2}. Rolling of the leukocyte is modeled by a rotation of the ellipse by the angle α, which is obtained by multiplying Λ with the orthonormal rotation matrix

$$\boldsymbol{R} = \begin{bmatrix} \cos(\alpha) & \sin(\alpha) \\ -\sin(\alpha) & \cos(\alpha) \end{bmatrix}. \tag{2}$$

This yields $\boldsymbol{c}^{\mathrm{T}} \boldsymbol{M} \boldsymbol{c} = 1$ with $\boldsymbol{M} = \boldsymbol{R}^{\mathbf{T}} \Lambda \boldsymbol{R}$. When the coordinates $\boldsymbol{b} = (x_0, y_0)^{\mathrm{T}}$ specify the centroid of the leukocyte, one obtains the general ellipse equation

$$(\boldsymbol{c} - \boldsymbol{b})^{\mathrm{T}} \boldsymbol{M} (\boldsymbol{c} - \boldsymbol{b}) = 1 \tag{3}$$

which we use to characterize the contour of a leukocyte. Equation (3) can be rewritten as

$$a(x - x_0)^2 + k(y - y_0)^2 + q(x - x_0)(y - y_0) = 1 \tag{4}$$

[1]Henceforward, c denotes a variable, $f(\cdot)$ a function, $\boldsymbol{c}$ a vector, C the Fourier transform of $\boldsymbol{c}$, $\boldsymbol{C}$ a matrix, $\underline{\boldsymbol{C}}$ the Fourier transform of the matrix $\boldsymbol{C}$ and the complex conjugate of $\overline{\boldsymbol{C}}$. The notation $\boldsymbol{S}(j)$ denotes matrix j in a sample, the superscript ^{T} the vector or matrix transpose.

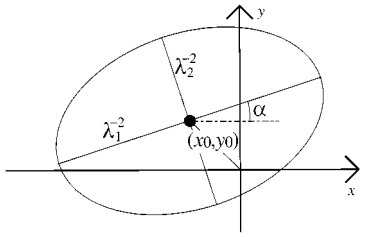

Fig. 2. The ellipse model consists of parameters specifying the length of the long (λ_1^{-2}) and short axes (λ_2^{-2}), the rotation angle (α) of the ellipse, and its center (x_0, y_0).

with

$$\begin{aligned} a &= \lambda_1 \cos(\alpha)^2 + \lambda_2 \sin(\alpha)^2 \\ k &= \lambda_1 \sin(\alpha)^2 + \lambda_2 \cos(\alpha)^2 \\ q &= 2(\lambda_1 - \lambda_2) \cos(\alpha) \sin(\alpha). \end{aligned} \tag{5}$$

Fig. 2 illustrates the parameters in the ellipse equation.

Define the *ellipticity* of the leukocyte

$$E \equiv \sqrt{\frac{\left(\lambda_1^{-2} - \lambda_2^{-2}\right)^2}{\left(\lambda_1^{-2} + \lambda_2^{-2}\right)^2}} \tag{6}$$

which specifies the relationship between the length of the long and short axes ($E = 0$ for a circle). The size of a leukocyte is defined by $l \equiv \frac{1}{2}(\lambda_1^{-2} + \lambda_2^{-2})$

$$\begin{bmatrix} p_x \\ p_y \end{bmatrix} = \left[\begin{bmatrix} \lambda_1 & 0 \\ 0 & \lambda_2 \end{bmatrix} \begin{bmatrix} \cos(\alpha) & \sin(\alpha) \\ -\sin(\alpha) & \cos(\alpha) \end{bmatrix} \right]^{\mathrm{T}} \begin{bmatrix} \cos(\phi) \\ \sin(\phi) \end{bmatrix} + \begin{bmatrix} x_0 \\ y_0 \end{bmatrix} \tag{7}$$

specifies the parametric coordinates $\boldsymbol{p} = (p_x, p_y)^{\mathrm{T}}$ along the ellipse as a function of the angle ϕ, with $\phi \in (0, 2\pi)$ the parametric variable.

C. Leukocyte Dimensions

To analyze the variation in size and ellipticity of leukocytes appearing in our image material, in total 120 leukocytes were manually detected in different images selected at random from the five grabbed video sequences. Around each leukocyte, a quadratic (30 × 30) window was extracted and its average intensity μ subtracted from the 900 pixel intensities. As the image gradient is large where the (bright) cytoplasm and the (dark) envelope meet, a SOBEL (gradient) operator [24] was applied on the extracted leukocyte image. From the gradient image, we obtained the coordinates of the n pixels that exceeded an automatically chosen threshold (see below). These coordinates were represented by the matrix

$$\boldsymbol{O} = \begin{bmatrix} x_1^2 & y_1^2 & x_1 y_1 \\ & \cdots & \\ x_n^2 & y_n^2 & x_n y_n \end{bmatrix}. \tag{8}$$

Each row in $\boldsymbol{O}$ specifies the coordinates of a pixel on the envelope of a leukocyte. For each leukocyte, a least mean square fit of its three parameters, $\hat{a}$, $\hat{k}$, and $\hat{q}$, is computed from

$$\begin{pmatrix} \hat{a} \\ \hat{k} \\ \hat{q} \end{pmatrix} = (\boldsymbol{O}^{\mathrm{T}}\boldsymbol{O})^{-1}\boldsymbol{O}^{\mathrm{T}}\boldsymbol{e} \tag{9}$$

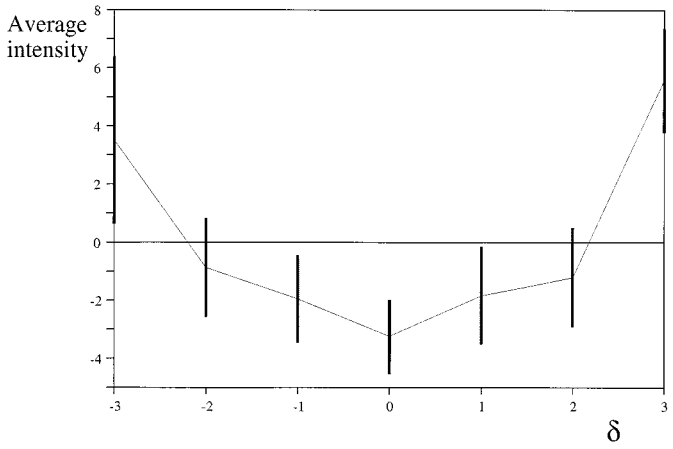

Fig. 3. The average intensity along the concentric ellipses is darkest around the membrane band, $\delta = 0$. The bars indicate the standard derivation measured among the 120 leukocytes.

with the vector $\boldsymbol{e} = (1, \ldots, 1)^{\mathrm{T}}$ having the length n. The threshold was chosen such that the average residual variation per coordinate pair

$$error = n^{-1} \left| \begin{pmatrix} \hat{a} \\ \hat{k} \\ \hat{q} \end{pmatrix} \boldsymbol{O} - \boldsymbol{e} \right| \tag{10}$$

was minimal, s.t. $n \geq 10$. $|\cdot|$ denotes the Euclidean vector norm. Note that $error = 0$ when all coordinate pairs in $\boldsymbol{O}$ lie on the ellipse specified by the parameters $\hat{a}$, $\hat{k}$ and $\hat{q}$. The eigenvalues Λ of the matrix

$$\boldsymbol{M} = \begin{bmatrix} \hat{a} & \hat{q}/2 \\ \hat{q}/2 & \hat{k} \end{bmatrix} \tag{11}$$

specify the dimensions of the leukocyte and the eigenvectors $\boldsymbol{R}$ its rotation angle α, $r_{1,1} = \cos(\alpha)$ and $r_{1,2} = \sin(\alpha)$.

Let $j = 1, \ldots, 120$ denote the index of a leukocyte in the sample. The parameters of each of the 120 manually detected leukocytes were computed as sketched above with $\lambda_1(j)$ and $\lambda_2(j)$ the estimated length of the long and short axes, and $\alpha(j)$ the rotation angle.

D. Envelope Band

To obtain statistical information of the intensity distribution of the envelope that separates a leukocyte from the surrounding blood, we investigated the intensity distribution of four cross sections of the cell membrane in each of the 120 leukocyte images. The average intensity was computed along the seven concentric, adjacent ellipses that jointly constitute the envelope band of each leukocyte. The size of each of these seven ellipses is given by the parameter δ and the parameters of the fitted ellipse, $(\lambda_1(j))^{-2} - (\delta - 1)$ and $(\lambda_2(j))^{-2} - (\delta - 1)$, with $\delta = -3, -1, \ldots, 3$. The intensity of the pixels is computed along the four cross sections parallel to the x and y axes in each image. Fig. 3 depicts the average intensity of each elliptic contour. The figure shows an initial decrease in intensity followed by a steep increase as a function of the distance in pixels to the ellipse with the minimal average intensity ($\delta = 0$).

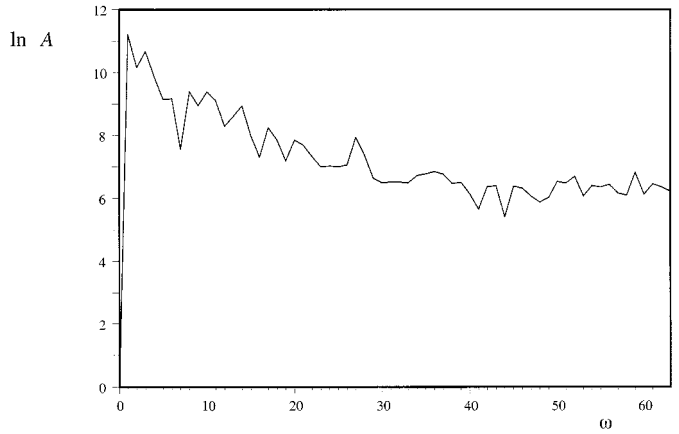

Fig. 4. Log magnitude spectrum of the 1-D autocorrelation function describing the intensity variation along the ellipse with the darkest average intensity in the membrane band, $\delta = 0$.

The intensity along the envelope band varies when, e.g., a leukocyte sticks to the vessel wall or is occluded by erythrocytes. The stochastic model we build should also take into account this intensity variation along the envelope band. We analyzed the intensity distribution of the ellipse with the lowest average intensity (intersecting the point $\delta = 0$ in Fig. 3) as a function of the angle ϕ [see (7)]. Let the vector $\boldsymbol{g}$ denote the intensities as a function of $\phi = 0, 2\pi/128, \ldots, 2\pi$. We computed the following statistics: the mean $\mu_{\boldsymbol{g}(j)}$ and variance $\sigma^2_{\boldsymbol{g}(j)}$ of the envelope distribution of leukocyte j as well as the autocorrelation function among the observations contained in $\boldsymbol{g}(j)$. This function characterizes correlations between neighboring pixels lying on the contour of the leukocyte.

First, the average gray value $\mu_{g(j)}$ is subtracted from $\boldsymbol{g}(j)$. Subsequently, the discrete Fourier transform is computed, $G(j) = \mathcal{F}\{\boldsymbol{g}(j)\}$. Multiplication with its complex conjugate results in the one-dimensional (1-D) autocorrelation function

$$A(j) = \mathcal{F}\{\boldsymbol{g}(j)\} \cdot \overline{\mathcal{F}\{\boldsymbol{g}(j)\}}. \tag{12}$$

This function characterizes the correlation between pixels with a radial distance of γ, 2γ, 3γ, …, 128γ with $\gamma = 2\pi/128$.

To obtain parameters that characterize the envelope intensity distribution of the whole sample of leukocyte images, we computed the average autocorrelation function $A = 120^{-1} \sum_{j=1,\ldots,120} A(j)$. Fig. 4 shows that the magnitude of the Fourier transform of the autocorrelation function A is prevailed by lower frequencies.

E. Cytoplasm Texture

Most of the pixels in a leukocyte image are part of the cytoplasm texture. To characterize this texture, we computed the frequency spectra from the 120 leukocyte images as follows. In each leukocyte image, we estimated the mean $\mu_{cy}(j)$ and variance $\sigma^2_{cy}(j)$ of the pixels inside the ellipse with the darkest average intensity. The mean $\mu_{cy}(j)$ was subtracted from those pixels, which were added to an image with the dimensions 32×32 that contained only zeros. The resulting image $\boldsymbol{T}(j)$ was rotated such that the long axis of the ellipse was parallel to the x-axis. This image was Fourier transformed and multiplied with its complex conjugate

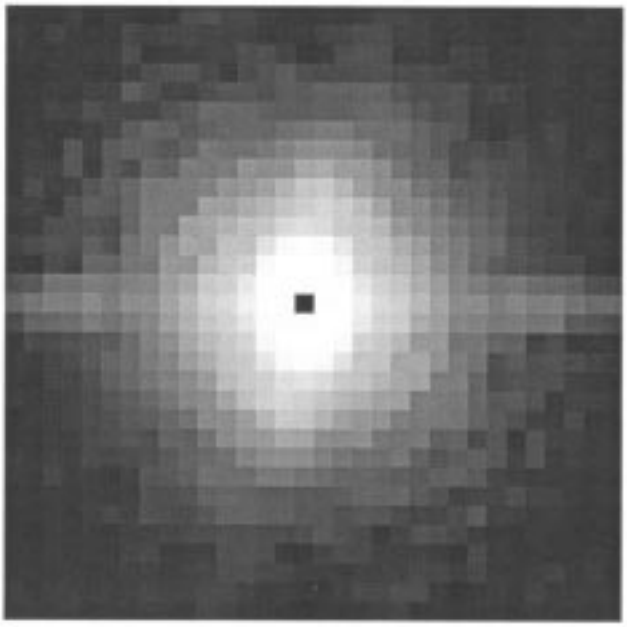

Fig. 5. Log magnitude spectrum of the 2-D autocorrelation function describing the frequency components of the cytoplasm texture. The autocorrelation function was computed from 120 leukocyte images.

$$\underline{D}(j) = \mathcal{F}_2\{\boldsymbol{T}(j)\} \cdot \overline{\mathcal{F}_2\{\boldsymbol{T}(j)\}} \tag{13}$$

with $\mathcal{F}_2$ denoting the two-dimensional (2-D) discrete Fourier transform. The average autocorrelation function of the cytoplasm texture $\underline{D}$ was computed from the 120 analyzed images, see Fig. 5.

F. Background Texture

An analysis of the frequency spectrum of the background (vessel) texture was also performed with 30 images that had been extracted from positions in the grabbed video images that contained no leukocytes. We computed the mean $\mu_{ba}(j)$ and variance $\sigma^2_{ba}(j)$ of each background image as well as the autocorrelation function as explained in the previous subsection. The spectrum of the background texture is prevailed by low frequencies, especially along the direction of flow.

G. Population Parameters

The 120 extracted leukocytes vary in size, brightness, and contrast, which we characterized by the following statistical parameters:

Shape and envelope distribution:

1) The average μ_E and variance σ^2_E *ellipticity*, the average μ_l and variance σ^2_l *size* among the 120 leukocytes.
2) The autocorrelation function A of the envelope distribution. The average μ_{μ_E} and variance $\sigma^2_{\mu_{\boldsymbol{g}}}$ of the envelope distribution *mean* $\mu_{\boldsymbol{g}}(j)$. The mean $\mu_{\sigma^2_{\boldsymbol{g}}}$ and variance $\sigma^2_{\sigma^2_{\boldsymbol{g}}}$ of the envelope distribution *variance* $\sigma^2_{\boldsymbol{g}}(j)$.

Cytoplasm texture:

3) The autocorrelation function $\underline{D}$ of the cytoplasm texture. The average $\mu_{\mu_{cy}}$ and variance $\sigma^2_{\mu_{cy}}$ of the *mean* intensity $\mu_{cy}(j)$. The average $\mu_{\sigma^2_{cy}}$ and variance $\sigma^2_{\sigma^2_{cy}}$ of the *variance* of the cytoplasm texture intensity $\sigma^2_{cy}(j)$.

Background texture:

4) The average $\mu_{\mu_{ba}}$ and variance $\sigma^2_{\mu_{ba}}$ of the *mean* intensity $\mu_{ba}(j)$ of the background texture.

Finally, we computed also the covariance matrix $\boldsymbol{S}$ of the four parameters $E(j), l(j), \mu_{cy}(j)$, and $\mu_{ba}(j)$ among the 120 leukocytes.

III. Stochastic Model of Leukocytes

In this section, we compose a stochastic model of the 2-D intensity distribution of a leukocyte based on the elliptic contour model and the other statistics presented in the previous section. The stochastic model characterizes the intensity distribution along the cross section of the envelope band, the intensity distribution along the envelope band as well as the inner and outer textures of a leukocyte image. Based on this model, synthetic images of leukocytes are generated which will be used to train neural networks to detect these cells in the blood vessel.

A. Envelope Function

We define the so-called *envelope function*, which specifies the average intensity of a cross section of the membrane band (Fig. 3), as a sum of two hyperbolic tangent functions

$$\epsilon(\delta,\phi) \equiv s\ \tanh\big(\delta - \tau(\phi)\big) - u\ \tanh(\delta - 1). \tag{14}$$

The parameters s and u, $\text{sign}(s) = \text{sign}(u)$, determine the asymptotic intensities inside $\mu_{cy} = (s-u)$ as well as outside $\mu_{ba} = -(s-u)$ the leukocyte (these average intensities depend on the particular light conditions—the contrast—in the image material at hand). The minimal value taken by the envelope function $\epsilon(\cdot)$ in between the two asymptotes depends on the angle ϕ of the vector connecting the center of the leukocyte $\boldsymbol{b} = (x_0, y_0)^{\mathrm{T}}$ [see (7)] to a particular point $\boldsymbol{c} = (x,y)^{\mathrm{T}}$ on the contour of the leukocyte

$$\tan(\phi) = \frac{x - x_0}{y - y_0}. \tag{15}$$

We use the *envelope distribution* A defined in (12) to specify the intensity variation along the darkest concentric ellipse as a function of (x,y). For a given angle ϕ, the function $\tau(\phi)$ returns the value that satisfies the equation

$$\tau(\phi) = \underset{\delta}{\text{argmin}}\ \{\epsilon(\delta,\phi)\} = a_\phi \tag{16}$$

with the vector $\boldsymbol{a}$ being the inverse Fourier transform of the average 1-D autocorrelation function A multiplied with the vector V, $\boldsymbol{a} = \mathcal{F}^{-1}\{A \cdot V\}$, with $\cdot$ denoting the element-by-element product. The vector $\boldsymbol{a}$ is a stochastic realization of a convolution of the average autocorrelation function A with (Fourier transformed) white noise $V = \mathcal{F}\{\boldsymbol{v}\}$, $\boldsymbol{v}$ being a vector with 2^d ($d \in \mathbb{N}$) numbers drawn at random from the standard normal distribution. The stochastic component $\boldsymbol{v}$ ensures that synthetic leukocytes have different envelope distributions but all with a frequency spectrum resembling that of real leukocyte images. The average and variance of $\boldsymbol{a}$ are chosen at random from the normal distributions $\mu_{\boldsymbol{g}} \sim N(\mu_{\mu_{\boldsymbol{g}}}, \sigma^2_{\mu_{\boldsymbol{g}}})$ and $\sigma^2_{\boldsymbol{g}} \sim N(\mu_{\sigma^2_{\boldsymbol{g}}}, \sigma^2_{\sigma^2_{\boldsymbol{g}}})$.

The envelope function $\epsilon(\delta,\phi)$ needs to be transformed into cartesian coordinates (x,y). We combine the ellipse model (4) with the envelope function (14) into

$$\begin{aligned} e(x,y,x_0,y_0) = s\ \tanh(&a(x-x_0)^2 + k(y-y_0)^2 \\ &+ q(x-x_0)(y-y_0) - t(x,y,x_0,y_0)) \\ &- u\tanh(a(x-x_0)^2 + k(y-y_0)^2 \\ &+ q(x-x_0)(y-y_0) - 1) \end{aligned} \tag{17}$$

with

$$t(x,y,x_0,y_0) = \tau\left(\arctan\left(\frac{x-x_0}{y-y_0}\right)\right) \tag{18}$$

The envelope function $e(x,y,x_0,y_0)$ resembles the mexican hat function, though its depth as specified by $t(x,y,x_0,y_0)$ depends on ϕ. Fig. 6(a) shows the resulting 2-D intensity distribution obtained by combining the envelope function with a membrane distribution chosen at random.

The dimensions of the leukocyte, E and l, together with the average intensities of the cytoplasm and background textures, $\mu_{cy}(j)$ and $\mu_{ba}(j)$, are drawn at random from the normal distribution

$$\big(E(j), l(j), \mu_{cy}(j), \mu_{ba}(j)\big)^{\mathrm{T}} \sim N(\boldsymbol{\mu}, \boldsymbol{S}) \tag{19}$$

with $\boldsymbol{\mu} = (\mu_E, \mu_l, \mu_{\mu_{cy}}, \mu_{\mu_{ba}})^{\mathrm{T}}$ the mean and $\boldsymbol{S}$ the covariance matrix.

B. Cytoplasm and Background Textures

Artificial cytoplasm texture is generated by convolving Gaussian noise with the 2-D average autocorrelation function $\boldsymbol{D}$ [see (13)]

$$\boldsymbol{C} = \mathcal{F}_2^{-1}\{\underline{V} \cdot \underline{D}\} \tag{20}$$

with $\underline{V} = \mathcal{F}_2\{\boldsymbol{V}\}$, an image with h rows and columns, $h = 2^d$, $d \in \mathbb{N}$, containing (uncorrelated) numbers drawn at random from the standard normal distribution. Fig. 6(b) exemplifies artificial leukocyte texture that is computed this way.

Before adding the texture $\boldsymbol{C}$ [Fig. 6(b)] to the artificial leukocyte image depicted in Fig. 6(a), its pixel intensities are scaled by the randomly chosen variance $\sigma^2_{cy}(j) \sim N(\mu_{\sigma^2_{cy}}, \sigma^2_{\sigma^2_{cy}})$ thereby ensuring that the texture intensities obtain a realistic dispersion. Cytoplasm texture $\boldsymbol{C}$ is added to pixels (x,y) for which

$$a(x-x_0)^2 + k(y-y_0)^2 + q(x-x_0)(y-y_0) < 1. \tag{21}$$

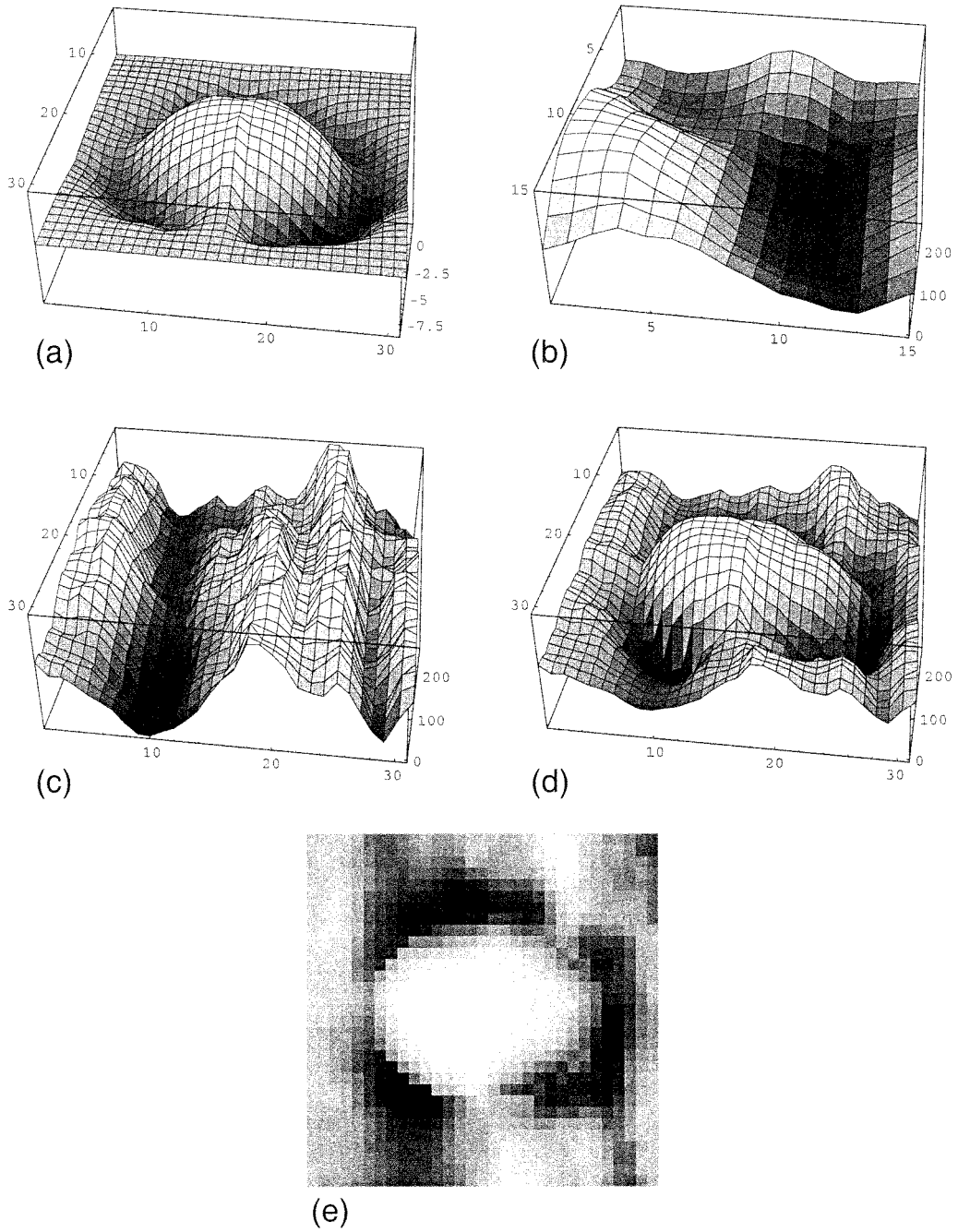

Fig. 6. This figure illustrates how an artificial leukocyte image is modeled from its constituent parts. (a) The envelope function and illustrates the effect of the membrane distribution. (b) The artificially generated cytoplasm texture of the cell image. (c) The background texture that is extracted from our image material. The two white tracks in the right-hand side indicate moving erythrocytes. (d) and (e) The leukocyte image generated by combining the information in (a), (b), and (c).

Because of the low frequency spectrum of the background texture in our image material, background textures $\boldsymbol{B}$ are drawn at random from the texture database (grabbed video images) rotated with a randomly chosen angle $\alpha \in (0, 2\pi)$ and added to pixels (x, y) in the leukocyte image for which

$$a(x - x_0)^2 + k(y - y_0)^2 + q(x - x_0)(y - y_0) \; > \; 1 \quad (22)$$

see Fig. 6(c) and (d).

C. Generating a Synthetic Leukocyte Image

Artificial images of leukocytes are generated with the stochastic model based on (17). The leukocyte model encompasses the following components.

- The dimensions of the leukocyte $E(j), l(j)$ and its rotation angle $\alpha(j)$. The coordinates of the leukocyte center $\boldsymbol{b}$ were always set to the central pixel of the image.
- The randomly chosen average intensities $\mu_{cy}(j)$ and $\mu_{ba}(j)$ that specify the contrast of the leukocyte images.

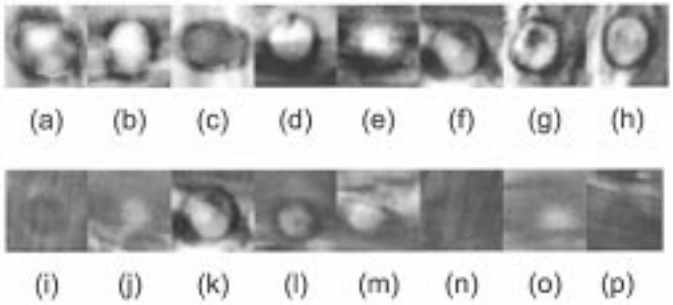

Fig. 7. (a)–(c) several examples of synthetic leukocyte images generated with our stochastic model, (d)–(h) leukocytes detected by both the best neural networks trained with synthetic and trained with real leukocyte images, (i)–(k) leukocytes only detected by the best "synthetic" neural network (leukocyte (i) is located centrally in the vessel), (l)–(m) leukocytes only detected by the best "real" neural network and (n)–(p) leukocytes that could not be detected by these two neural networks.

- The envelope distribution $\tau(\phi)$ given by the autocorrelation function $\boldsymbol{g}$ and its randomly chosen mean $\mu_{\boldsymbol{g}}(j) \sim N(\mu_{\mu_{\boldsymbol{g}}}, \sigma^2_{\mu_{\boldsymbol{g}}})$ and variance $\sigma^2_{\boldsymbol{g}}(j) \sim N(\mu_{\sigma^2_{\boldsymbol{g}}}, \sigma^2_{\sigma^2_{\boldsymbol{g}}})$.
- The cytoplasm and background textures, $\boldsymbol{C}$ and $\boldsymbol{B}$, the randomly chosen variance σ^2_{cy} of the cytoplasm texture, as well as the direction of flow, α_{flow}.

Fig. 6 shows the components of a synthetic leukocyte image and Fig. 7(a)–(c) examples of synthetic leukocyte images.

IV. Experiments

We performed two experiments. In the first experiment, the required size of the training set is determined. In the second experiment, the detection performance is compared between neural networks trained with real leukocyte images and trained with leukocyte images generated using the stochastic model.

A. Training Neural Networks for Leukocyte Detection

We first investigated whether feed-forward neural networks with one hidden layer could be trained to recognize white blood cells in the microcirculation images. To reduce the dimensionality of the input window with a factor of four, all video images were blurred with a circular symmetric Gaussian kernel ($\sigma^2 = 1$) and subsampled with a factor of two resulting in images with the size 96×192 pixels. Neural networks were subsequently trained to classify subimages (13×13 pixels) as leukocyte or background. A network should result in a high activation when the window is positioned on a leukocyte. Otherwise, the neural network should result in a small output value. The training set consisted of subimages containing either a leukocyte or background.

It has been shown that the fractions of patterns of the classes one wants to discern (background and leukocyte) should mimic the prior probabilities of observing the objects belonging to these classes in the image material [25]. When we assume that a leukocyte may be recognized when the window center is positioned within ± 1 pixel from the centroid of the leukocyte, a convolution operation will maximally result in five leukocyte detections per white blood cell. So all detections forming a group of eight-connected pixels are considered as positive evidence of one leukocyte. However, a single positive detection is considered sufficient positive evidence for a leukocyte. A normal vessel, which constitutes our region of interest, covers about $1/3$ of the image, i.e., 9000 pixels. Assuming further that a video image contains 10–20 leukocytes, five positive detections per leukocyte corresponds with a prior probability of about 1%, $P(\text{leukocyte}) = 0.01$.

Three different training sets were composed by drawing at random 2000, 5000, and 9000 subimages, 13×13 pixels, from the background available in our image database. The background images were solely taken from areas inside the vessel that contain no leukocytes; tissue outside the vessel was omitted from the training set. Then 20, 50, and 90 manually detected leukocyte images were added to the three training sets. To rule out the influence of the brightness of the leukocyte subimage, the average intensity of each subimage was set to zero. Feed-forward neural networks with different topologies were trained, $13 \times 13 - z - 2$, $z \in 7, \ldots, 12$, where z is the number of hidden nodes (networks with fewer than seven hidden nodes frequently ended up in poor local minima). The two required outputs were ($o_1 = 1, o_2 = 0$) for leukocytes and ($o_1 = 0, o_2 = 1$) when the training image contained background. The neural networks were trained with back-propagation [26], offline learning for maximally 3000 cycles, learning rate 0.0001 and momentum 0.5.

The experiment indicated that solely neural networks with the largest training set consisting of 9000 images generalized well on test images. A convolution with a video image containing 16 leukocytes followed by thresholding resulted in 10–15 true and 1–5 false detections depending on the chosen threshold value, $o_1 - o_2 > \kappa$. Reducing the fraction of leukocyte images in the training sets to less than 1% had the effect that the neural networks classified the whole vessel area as background.

B. Comparison of Neural Networks Trained with Artificial and Real Leukocyte Images

In this experiment, neural networks with the topologies $13 \times 13 - z - 2$, $z \in 7, \ldots, 12$, were trained with two training sets both consisting of 90 leukocyte and 9000 background images. In the first training set, the leukocyte images were generated with our stochastic model whereas the second training set contained 90 manually detected leukocyte images instead. In both training sets, the same 9000 background images were used as in the first experiment.

The performance of the neural networks was compared by computing receiver operating characteristic (ROC) curves [27]. A ROC curve depicts the fraction of true versus false positive detections for different values of a varying threshold. As performance measure, we computed the area under each ROC curve. This measure is independent of a particularly chosen threshold value.

The performance of the trained neural networks was tested on three microcirculation images, each from a different sequence, which had not been used to build the training set. Each neural network was used to detect leukocytes in the three test images. A threshold value κ was applied on the output of the neural network. Initially, the threshold was set so that as many as possible positive detections of leukocytes were obtained in the image

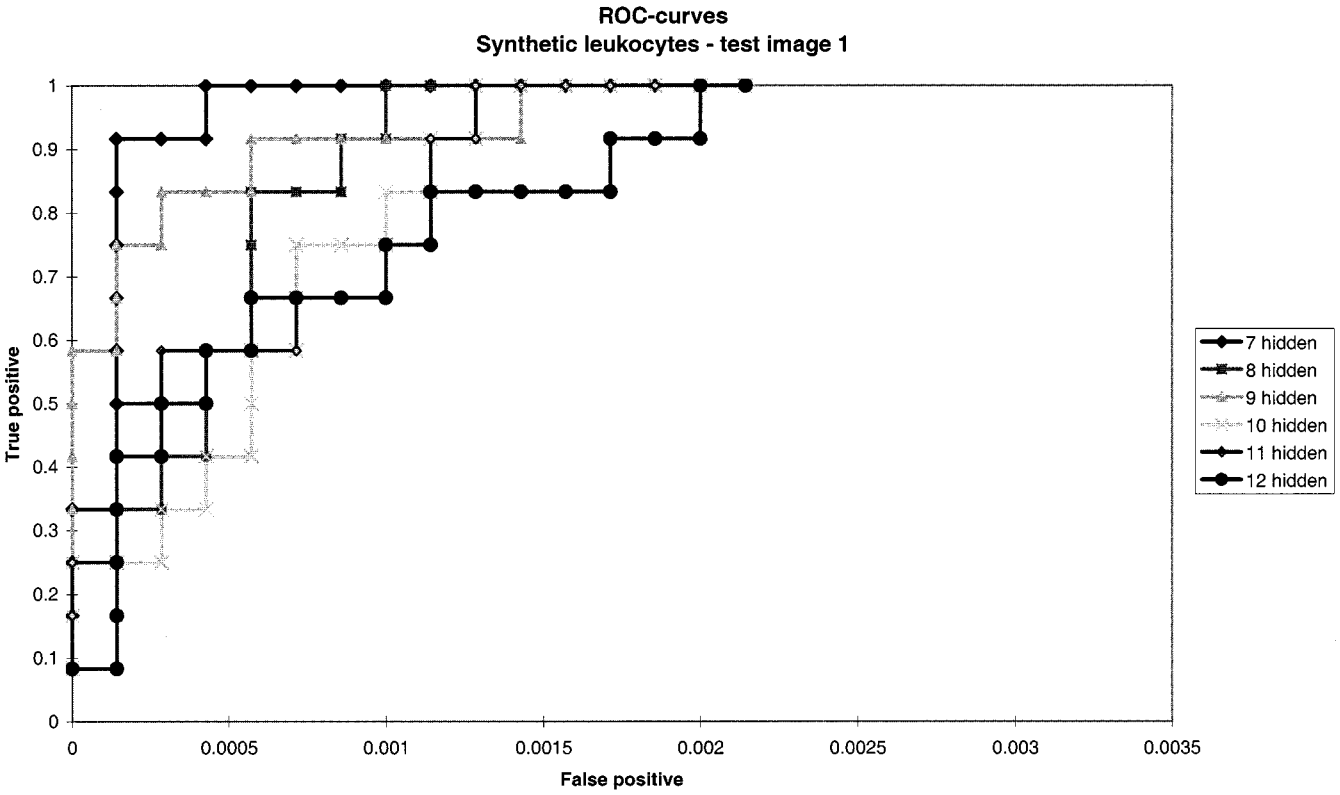

Fig. 8. ROC curves, test image 1, networks trained with artificial leukocyte images.

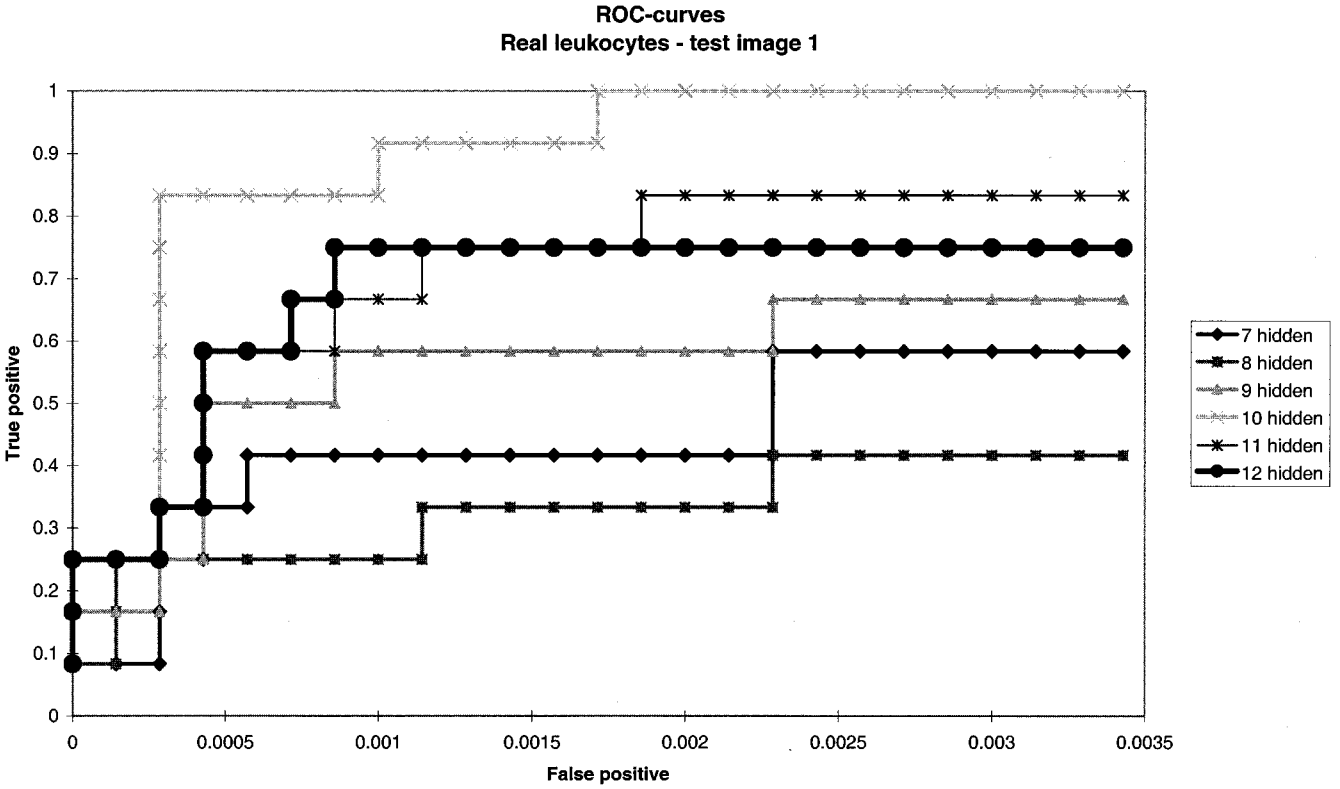

Fig. 9. ROC curves, test image 1, networks trained with real leukocyte images.

without making any false positive detections. Then the threshold was decreased step by step, each time allowing one more detection. Fig. 8 shows the resulting ROC curves of six different neural networks trained with artificially generated leukocyte im-

TABLE I
ROC INTEGRALS FOR EACH OF THE 12 NEURAL NETWORKS COMPUTED USING THE THREE TEST IMAGES

Hidden nodes	ROC-intergral of NN Artificial leykocytes			ROC-integral of NN Real leykocytes		
	Image 1	Image 2	Image 3	Image 1	Image 2	Image 3
7	0.965	0.519	0.828	0.434	0.534	0.463
8	0.875	0.549	0.867	0.326	0.774	0.561
9	0.938	0.947	0.800	0.552	0.789	0.438
10	0.837	0.767	0.783	0.885	0.571	0.608
11	0.854	0.872	0.772	0.701	0.835	0.583
12	0.813	0.737	0.700	0.674	0.820	0.469

ages. Fig. 9 depicts similar ROC curves for the networks trained with images of real leukocytes. Table I shows the areas under the ROC curves for the 12 neural networks (six trained with synthetic and six trained with real leukocyte images) applied on the three different test images.

The ROC curves clearly indicate that the neural networks trained with synthetic leukocyte images performed better than the networks trained with real leukocyte images. The networks with nine hidden nodes trained with the training set that contained the 90 artificially generated leukocyte images resulted in the best performance. The average area under the ROC curve is 0.90. The neural network with 11 hidden nodes performed best among those trained with real leukocyte images; its average ROC area is 0.71.

V. DISCUSSION

The neural networks trained with artificially generated leukocyte images perform better than those trained with real images. The neural networks with 9 hidden nodes trained with synthetic leukocyte images perform best on the test images, it has an 18% larger area under the ROC curve than the best network trained with real leukocyte images. Even leukocytes that interact with a part of the wall that is currently out of focus can be detected with the best neural networks, see Fig. 7(i) and (j).

The approach presented here can be useful for automatic detection and later tracking of leukocytes in microcirculation images. An overall indicator of leukocyte-endothelium interactions that can be computed automatically is the total number of interacting leukocytes per 100-μm vessel length. Estimates of the (change in) ellipticity E and size l of detected leukocytes can be used to characterize their deformation during rolling, adhesion and diapedesis. This deformation is closely related to the forces exerted on the leukocyte. However, a robust estimation of the geometric parameters E and l relies on a good thresholding of the SOBEL (gradient) image. In the future, more attention should be paid to improving this thresholding procedure.

In the future, the approach can be incorporated in a tracking algorithm for estimation of the rolling velocity of individual leukocytes. A pilot experiment has indicated that the estimated ellipticity and size of a leukocyte are features that lend themselves for determining whether leukocytes in successive images correspond. However, more information about the local direction of flow and the absolute leukocyte positions in successive images need to be taken into account. Sato *et al.* [2] present an interesting solution to the tracking problem based on Hopfield networks for coupling partial leukocyte traces.

VI. CONCLUSION

We presented an approach for detection and characterization of leukocytes in video images obtained from *in vivo* microcirculation experiments. Neural networks were trained to detect leukocytes using a training set consisting of images of leukocytes and of the background consisting of fast-moving erythrocytes in a venule. Two training sets were used. One consisted of a mixture of samples of background and leukocyte images, both extracted from different video images. In the second training set, we used synthetic leukocyte images which were generated using a novel stochastic model of the intensity distribution of a leukocyte. The model contains the following three components:

1) a membrane (envelope band) with an elliptic shape;
2) a cytoplasm texture;
3) a background texture.

The stochastic leukocyte model contains 14 parameters which we estimated from a sample consisting of 120 manually extracted leukocyte images. The experiments indicate that the neural networks trained with artificially generated leukocyte images obtained a better performance than networks trained with a sample of leukocyte images extracted from our image material. This principle for generation of synthetic samples may be useful for training neural networks for object detection in other applications.

Our detection approach is interesting for automatically processing video images from microcirculation experiments. Besides aiding automatic computation of the number of interacting leukocytes per unit vessel length, the deformation of leukocytes during rolling, adhesion or diapedesis may be quantified using geometric parameters.

A subject for future research is to incorporate our detection algorithm in an approach for tracking of individual leukocytes. Thereby, special attention should be paid to the development of

a method for automatically thresholding the output image from the convolution neural network in order to recognize as many leukocytes as possible but omitting most false positive detections. Another issue is how to combine the geometric information (size and ellipticity) of each leukocyte with information on the direction of flow in such a tracking approach.

REFERENCES

[1] M. G. A. oude Egbrink, G. J. Tangelder, D. W. Slaaf, and R. S. Reneman, "Influence of platelet-vessel wall interactions on leukocyte rolling *in vivo*," *Circ. Res.*, vol. 70, no. 2, pp. 355–363, 1992.

[2] Y. Sato, J. Chen, R. A. Zoroofi, N. Harada, S. Tamura, and T. Shiga, "Automatic extraction and measurement of leukocyte motion in microvessels using spatiotemporal image analysis," *IEEE Trans. Biomed. Eng.*, vol. 44, pp. 225–236, Apr. 1997.

[3] J. Hektor, J. Jansen, H. Heidtmann, H. Schmid-Schönbein, and R. Grebe, "A setup for computer-assisted tracking of erthrocytes in microvascular networks," *J. Computer-Assisted Microscopy*, vol. 9, no. 3, pp. 135–141, 1997.

[4] M. Watanabe, Y. Senga, T. Shiga, and S. Miname, "The time-space correlation method for measurement of erythrocyte velocity in microvessels using a CCD linear imaging sensor," *Microvasc. Res.*, vol. 41, pp. 41–46, 1991.

[5] C. Y. J. Yip, Y. Aggerwal, K. R. Diller, and S. C. Bovik, "Simultaneous multiple site arteriolar vasomotion measurement using digital image analysis," *Microvasc. Res.*, vol. 41, pp. 73–83, 1991.

[6] M. Egmont-Petersen and T. Arts, "Recognition of radiopaque markers in X-ray images using a neural network as nonlinear filter," *Pattern Recogn. Lett.*, vol. 20, no. 5, pp. 521–533, 1999.

[7] R. C. Gonsalez and R. E. Woods, *Digital Image Processing*. Reading, MA: Addison-Wesley, 1992.

[8] M. Egmont-Petersen and T. Arts, "Detection of implanted markers in radiographic image sequences," in *Aachener Workshop für Bildverarbeitung in der Medizin (Aachen Workshop on Medical Image Processing)*, T. Lehmann and K. Spitzer, Eds, Germany: Aachen, 1996, pp. 209–214.

[9] D. DeKruger and B. R. Hunt, "Image processing and neural networks for recognition of cartographic area features," *Pattern Recognition*, vol. 27, no. 4, pp. 461–483, 1994.

[10] M. Egmont-Petersen and E. Pelikan, "Detection of bone tumours in radiographs using neural networks," *Pattern Anal. Applicat.*, vol. 2, no. 2, pp. 521–533, 1999.

[11] M. Kass, A. Witkin, and D. Terzopoulos, "Snakes: Active contour models," *Int. J. Comput. Vision*, pp. 321–331, 1988.

[12] S. Lobregt and M. A. Viergever, "A discrete dynamic contour model," *IEEE Trans. Med. Imag.*, vol. 14, pp. 12–24, Feb. 1995.

[13] C. Vieren, F. Cabestaing, and J.-G. Postaire, "Catching moving objects with snakes for motion tracking," *Pattern Recogn. Lett.*, vol. 16, pp. 679–685, 1995.

[14] T. F. Cootes, C. J. Taylor, D. H. Cooper, and J. Graham, "Active shape models—Their training and application," *Comput. Vision Image Understanding*, vol. 61, no. 1, pp. 38–59, 1995.

[15] A. Califano and R. Mohan, "Multidimensional indexing for recognizing visual shapes," *IEEE Trans. Pattern Anal. Machine Intell.*, vol. 16, pp. 373–392, Apr. 1994.

[16] T. M. Cover and P. E. Hart, "Nearest neighbor pattern classification," *IEEE Trans. Inform. Theory*, vol. IT-13, pp. 21–27, Jan. 1967.

[17] K.-I. Funahashi, "On the approximate realization of continuous mappings by neural networks," *Neural Networks*, vol. 2, pp. 183–192, 1989.

[18] K. Hornik, "Approximation capabilities of multilayer feedforward networks," *Neural Networks*, vol. 4, pp. 251–257, 1991.

[19] J. D. Villiers and B. Bernard, "Backpropagation neural nets with one and two hidden layers," *IEEE Trans. Neural Networks*, pp. 136–141, July 1992.

[20] M. D. Richard and R. P. Lippmann, "Neural network classifiers estimate bayesian a posteriori probabilities," *Neural Computation*, vol. 3, pp. 461–483, 1991.

[21] T. A. Springer, "Traffic signals for lymphocyte recirculation and leukocyte emigration: The multistep paradigm," *Cell*, vol. 76, pp. 301–314, 1994.

[22] D. W. Slaaf, R. Alewijnse, and H. Wayland, "Use of telescopic imaging in intravital microscopy: A simple solution for conventional microscopes," *Int. J. Microcirc.; Clin. Exp.*, vol. 1, pp. 121–134, 1982.

[23] T. Lindeberg and B. M. ter Haar Romeny, "Linear scale-space theory," in *Geometry-Driven Diffusion in Computer Vision*, B. M. ter Haar Romeny, Ed. Dordrecht, The Netherlands: Kluwer Academic, 1994, ch. 2.

[24] B. Jähne, *Digital Image Processing. Concepts, Algorithms and Scientific Applications*. Berlin, Germany: Springer-Verlag, 1995.

[25] D. H. Wolpert and W. G. Macready, "No free lunch theorems for search," The Santa Fe Institute, Santa Fe, NM, Tech. Rep. SFI-95-02-010, 1995.

[26] D. E. Rumelhart, G. E. Hinton, and R. J. Williams, "Learning internal representations by error propagation," in *Parallel Distributed Processing. Exploration into the Microstructure of Cognition*, D. E. Rumelhart and J. L. McClelland, Eds. Cambridge, MA: MIT Press, 1986, vol. 1, pp. 318–364.

[27] M. C. Weinstein, H. V. Fineberg, A. S. Elstein, H. S. Frazier, D. Neuhauser, R. R. Neutra, and B. J. McNeil, *Clinical Decision Analysis*. Philadelphia, PA: Saunders, 1978.

M. Egmont-Petersen was born in Copenhagen, Denmark, in 1967. He received the combined B.S. and combined M.S. degrees in computer science/business administration from Copenhagen Business School, Copenhagen, Denmark, in 1988 and 1990, respectively. He received the Ph.D. degree in medical informatics from Maastricht University, Maastricht, The Netherlands, in 1996.

He is currently with the Division of Image Processing, Department of Radiology, Leiden University Medical Center, Leiden, The Netherlands, as Postdoctoral Researcher. He is currently working with the quantification of perfusion in bone tumors based on dynamic MRI. His main research interests include neural networks, support vector machines, statistical classifiers, feature selection, quality assessment of classifiers, nonlinear filtering, object detection, and invariant theory. He has published more than 30 papers in scientific journals and conference proceedings.

Dr. Egmont-Petersen is a member of the IEEE Computer Society, the Dutch society for Pattern Recognition and Image Processing, and Working Group TC9 (Biomedical Pattern Recognition) under the auspices of ICPR.

U. Schreiner was born in Wegberg, Germany, in 1972. He received the M.S. degree in computer science from the University of Technology (RWTH), Aachen, Germany, in 1998.

He is currently with the Debis Systemhaus-Services by DaimlerChrysler and is working as Project Developer/Manager in the Department of Health and Social Services. He develops solutions for hospitals and healthcare associations.

S. C. Tromp was born in Hellendoorn, the Netherlands in 1971. She received the M.D. degree at the Faculty of Medicine of Maastricht University, Maastricht, The Netherlands, in March 1999 and the Ph.D. degree in medical physiology from Maastricht University in December 1999. Her Ph.D. dissertation concerns *in vivo* modulation of leukocyte-endothelium interactions.

She is currently a Junior Resident in the Department of Neurology, at the University Hospital Maastricht, the Netherlands. Her research interests include the role of mast cells, prostaglandins, and angiogenic factors in induction and inhibition of leukocyte rolling and/or adhesion. Furthermore, the influence of a thromboembolic reaction on leukocyte-endothelium interactions in the microcirculation is studied.

T. M. Lehmann (S'94–M'99) received the M.S. degree in electrical engineering and the Ph.D. degree (*summa cum laude*) in computer science from the Aachen University of Technology (RWTH), Aachen, Germany, in 1992 and 1998, respectively.

In 1992 he was a Research Scientist at the Faculty of Electrical Engineering, RWTH. Since 1992, he is with the Institute of Medical Informatics, Medical Faculty, RWTH, where he currently heads the Department of Medical Image Processing as Assistant Professor. He co-authored a textbook on image processing for the medical sciences which has been published by Springer-Verlag, Berlin, Germany. His research interest are discrete realizations of continuous image transforms, medical image processing applied to quantitative measurements for diagnoses and content-based image retrieval from large databases.

In 1993, Dr. Lehmann received the DAGM-Preis '93. He received an award from the German Association for Pattern Recognition for his work on automatic strabometry using Hough transform and covariance filtering. In 1998, he received the Borcher's Medal from the RWTH Aachen for his work on medical image registration. He is the Chairman of the German Workshop on Medical Image Processing and Vice-President of the working group Medical Image Processing within the German Society of Medical Informatics, Biometry and Epidemiology (GMDS). He is a member of the International Association of Dentomaxillofacial Radiology (IADMFR) and the Society of Photo-Optical Instrumentation Engineering (SPIE).

D. W. Slaaf was born in 1945. He studied experimental physics at the University of Utrecht, The Netherlands, where he graduated in 1972. He received the PhD degree in electrophysiology from the same university in 1977.

He joined the Department of Biophysics of the Universiteit Maastricht, Maastricht, The Netherlands, in 1975, was appointed Associate Professor of Biophysics in 1979, and Professor of Physics of the Microcirculation in 1997. He was actively involved in the development of the microcirculation program in the laboratory and the clinic. In 1991 he was appointed Adjunct Professor at the University of Louisville, Louisville, KY. Currently he combines his research at the Universiteit Maastricht with his role of Vice-Dean of the Faculty of Biomedical Engineering of the Technical University of Eindhoven. He is author or co-author of over 150 papers and book chapters.

T. Arts received the M.Sc. degree in electronical engineering at Eindhoven University of Technology, Eindhoven, The Netherlands, in 1971. In 1978, he received the Ph.D. degree in medicine at Maastricht University, Maastricht, The Netherlands, in the field of cardiac mechanics.

He received a five-year appointment to the Department of Mechanical Engineering at Eindhoven University of Technology. Currently he is Associate Professor with the Department of Biophysics, Maastricht University, and full Professor with the Faculty of Mechanical Engineering, Eindhoven University of Technology. His main research interests are modeling and experimenting in cardiovascular mechanics, constitutive relations of cardiovascular tissues, changes due to adaptive remodeling, and measuring and analysis methods of motion and deformation in optical, X-ray and MRI image sequences.